

Phosphazene catalyzed addition to electron-deficient alkynes: the importance of non-linear allenyl intermediates upon stereoselectivity.

Luis Simón^{†}, Robert S. Paton^{*‡}*

[†] Facultad de Ciencias Químicas, Universidad de Salamanca, Plaza de los Caídos 1-5, Salamanca E37004, Spain.

[‡] Chemistry Research Laboratory, University of Oxford, Mansfield Road, Oxford OX1 3TA, UK.

KEYWORDS

DFT calculations; reaction mechanism; Organocatalysis; Phosphazene catalysts; diiminophosphorane catalysts; Superbases; Alkyne Addition; Z/E selectivity.

ABSTRACT

An ONIOM(QM/MM) study on the mechanism of the Michael addition to triple bonds catalyzed by chiral diiminophosphorane catalysts has been performed to understand the stereoselectivity of the product olefin. Our results are consistent with the experimental enantioselectivity, but more importantly, reveal that the *Z* vs *E* preference depends on the influence of the catalyst upon the

geometry of the allenyl enolate formed in the addition step. These intermediates show an innate preference for a (*Z*)-configuration, although this can be suppressed by steric interactions due to a catalyst. This leads to two distinct mechanisms in which the kinetic basis for (*E*) or (*Z*)-stereoselectivity is determined by a different step. Bifunctional iminophosphorane catalysts are found to use steric interactions to override innate stereoelectronic effects of the allenyl enolate reactive intermediate.

Introduction

The scope of nucleophilic addition to electron-deficient double bonds (i.e. Michael addition) has been broadened by the development of asymmetric organocatalysis.¹⁻¹⁹ The analogous addition to conjugated alkynes is a potentially useful transformation, yielding a substituted vinylic system that can be further modified.²⁰ Control of the alkene *E/Z*-stereochemistry is essential for such a reaction; however, stereoselective organocatalytic examples are relatively scarce. With nucleophilic organocatalysts such as tertiary amines²¹⁻²³ or phosphines,²³⁻²⁵ the thermodynamically more stable (*E*)-olefin product dominates. A similar result is obtained with phase-transfer organocatalysts developed by Maruoka.²⁶⁻²⁸ In contrast, using hydrogen-bonding organocatalysts, both diastereomers have been obtained: Misaki and Sugimura²⁹ reported a highly *Z*-selective addition of azlactones to alkynones catalyzed by chiral guanidines, while You disclosed a highly *E*-selective Hantzsch-ester reduction of alkynylimino-derivatives catalyzed by a chiral phosphoric acid (CPA)³⁰.

The addition of azlactones³¹ and 2-benzyloxythiazol-5(4 H)-ones³² to electron-deficient alkynes catalyzed by chiral iminophosphoranes has been developed by Ooi and co-workers. Four

stereoisomeric adducts are possible since the use of a prochiral enolate results in the creation of a new stereogenic center along with alkene formation. Ooi has shown that it is possible to obtain excellent E/Z selectivity, but even more remarkably, that this selectivity can be reversed by small changes made to the electrophile or catalyst (**Figure 1**).

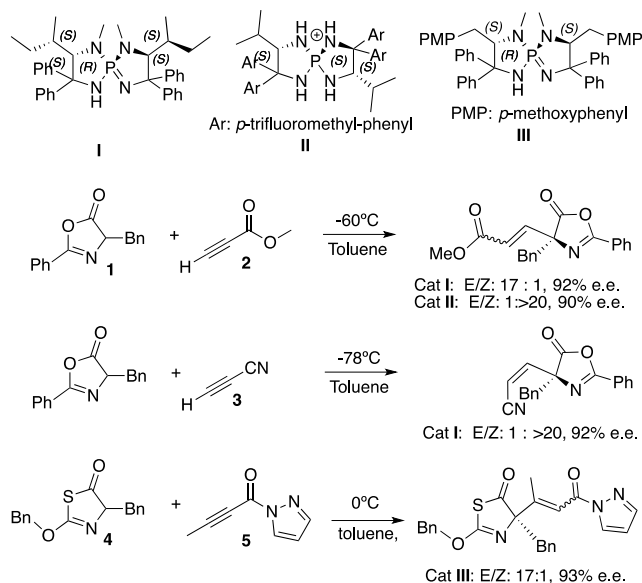


Figure 1. Iminophosphorane catalyzed additions of azlactones and 2-benzyloxythiazol-5(4H)-ones to electron-deficient alkynes.

Chiral iminophosphorane organocatalysts show catalytic activity and enantioselectivity³³ in reactions in which their high basicity allows them to activate pro-nucleophiles by deprotonation, including nitroalkanes,³⁴⁻³⁸ dialkyl phosphonates,³⁹⁻⁴¹ thiols,⁴² azlactones,⁴³⁻⁴⁵ dithianes,⁴⁶ thiolactones,⁴⁷ oxindoles,⁴⁸⁻⁵⁰ and ketones.⁵¹

Understanding how chiral counterions exert a stereocontrolling influence solely through noncovalent interactions is an area of intense interest from both experimental⁵² and theoretical^{53,54} perspectives. Recently, we computed the mechanism of nitro- and phospho-aldol

reactions catalyzed by bis-iminophosphoranes.⁵⁵ These calculations show that, after deprotonating the nucleophile, the catalyst forms hydrogen-bonds with both reactants to control the stereo-determining transition structure (TS) geometry. More recently, Yamanaka and Ooi have published⁵⁶ a theoretical study on the mechanism of the 1,6-addition of azlactones to dienyl N-acylpyrroles, again observing dual activation of both reactants by the catalyst. We now describe our studies on the mechanism of addition to activated triple bonds catalyzed by iminophosphorane catalysts. Since the thermodynamically less-stable diastereomer is formed using different combinations of substrate and catalyst, we sought to establish the kinetic basis for stereoselectivity.

The addition consists of two elementary steps: C-C bond formation and then protonation. Three distinct mechanistic scenarios were envisaged to account for stereocontrol. One possibility which reflects previous proposals is the irreversible C-C formation as the enantiodetermining step, followed by irreversible protonation of a linear allenyl intermediate as the diastereodetermining step (**Figure 2a**). It was also proposed that diastereoselectivity is dependent upon whether enolate protonation occurs at O (with a subsequent 1,3 H shift to afford the thermodynamically more stable (*E*)-product) or directly at C, yielding the (*Z*)-product. Additionally, we considered the possibility of a scenario in which C-C bond formation is reversible whereas enolate protonation is irreversible. In this case, this second step is both enantio- and diastereo-determining (**Figure 2b**). Finally, based on the hypothesis that the intermediates are non-linear, and non-interconverting, we considered a third possibility in which C-C bond formation is both enantio and diastereo-determining (**Figure 2c**). As we shall discuss, we find that kinetically-controlled (*Z*)-selectivity is characteristic of the first scenario, and (*E*)-selectivity results from the third.

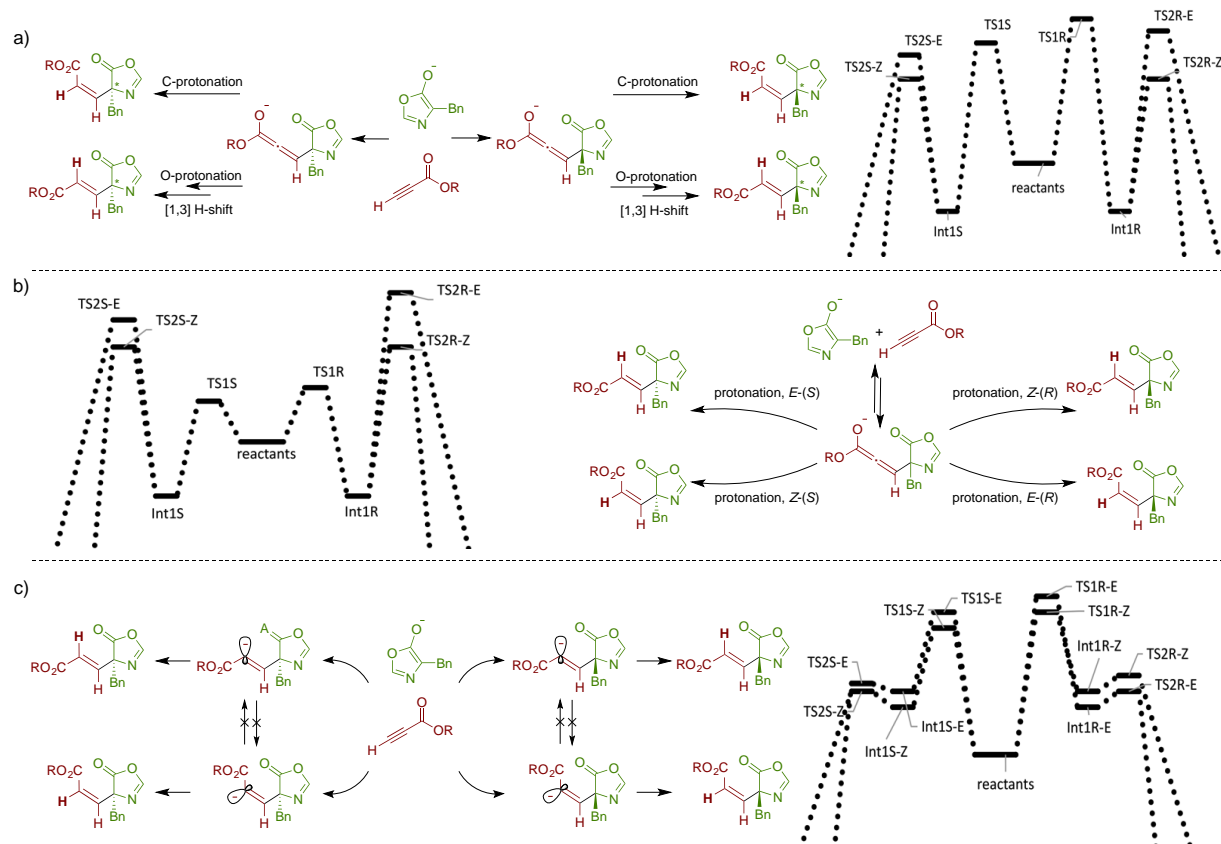


Figure 2. Distinct mechanistic possibilities for enantio- and diastereo-control: a) the Michael addition is enantiocontrolling and protonation is diastereocontrolling; b) Michael addition is reversible and enantio- and diastereoselectivity are both controlled by irreversible protonation; c) Michael addition is irreversible and controls both enantio- and diastereoselectivity, since protonation of carbanion intermediates is faster than their interconversion. Energy diagrams are illustrative and do not correspond to results of the calculations.

Computational methods

Calculations were performed using the *Gaussian09* program.⁵⁷ Geometry optimizations and vibrational frequencies were computed at the ONIOM(QM/MM) level of theory using the

ONIOM implementation.⁵⁸⁻⁶⁰ As we have discussed previously, a molecular mechanics (MM) layer is useful in describing large organocatalytic systems with multiple van der Waals interactions due to the presence of explicitly parameterized interatomic Lennard-Jones potentials.⁶¹ The quantum mechanics (QM) layer has been used to describe the core TS including breaking/forming bonds and substrate-catalyst hydrogen-bonds. The favorable cost of ONIOM(QM/MM) calculations has enabled all possible TS conformations to be systematically explored without resort to a simplified chemical model. This was performed manually, although substrate:catalyst modes can be explored in an automated fashion.⁵⁴ The partition of atoms into high and low-level layers is shown, in 3D structures, by “ball & stick” and “wireframe” representations, respectively, and in structural formulas atoms in the low-level layer are drawn in blue. The hybrid meta-GGA M06-2X^{62,63} density functional was used with the 6-31G(d,p)^{64,65} basis set in the QM high-level layer, and UFF⁶⁶ was used for the MM low-level layer. This force field has performed well in the description of catalytic reactions for which a rigid, hydrocarbon low-level layer interacts via non-bonding interactions with the rest of the structure.^{55,67-74} The ONIOM(QM:MM) TS geometries gave a good overlay with selected structures optimized at the M06-2X/6-31G(d,p) level for the full system (see SI section, figure S2). The RMSD between the structures are comparable with values obtained for TS structures optimized by different DFT functionals.⁷⁵ The use of a non-polar solvent (toluene) experimentally encourages tight ion-pairing between catalyst and substrate(s), and the effect of solvation on the optimized geometries is anticipated to be minimal.⁷⁶ Optimized structures were subjected to a M06-2X/6-311+G(d,p) single point energy evaluation;⁷⁷ the solvent (toluene) was modeled by means of an IEFPCM⁷⁸⁻⁸² method using the SMD universal solvation model⁸³ and solvent accessible surface (SAS) cavity. Thermal contributions to the Gibbs energies were obtained from vibrational frequencies in the

quasi-rigid rotor-harmonic oscillator (quasi-RRHO) approach as described by Grimme,⁸⁴ using a free-rotor approximation for anharmonic vibrational modes below 100 cm⁻¹ and a rigid rotor approximation above this cut-off for vibrational entropies.⁸⁵ Quantitative estimates of stereoselectivity have been performed according to the assumptions of transition state theory and upon application of the Curtin-Hammett principle: we assume rapid equilibration of diastereomeric pre-reactive complexes relative to bond-formation such that association is not stereo-determining. Only the relative free energies of competing transition structures are compared. Figures were prepared with *Pymol v0.99*.⁸⁶ Noncovalent interaction (NCI) indices were calculated with NCIPLOT.⁸⁷⁻⁸⁹ Steric maps are used to identify regions of the catalyst in which placement of the reagents incurs a steric penalty (Figures 4 and 7). These are inspired by Cavallo's steric maps⁹⁰⁻⁹²; however, since the catalysts studied here have two distinct interaction sites with the reagents, steric contacts are not localized within a sphere, but on planes parallel to the catalyst active site (see details in Supporting information and figure S1).

Results and discussion

We first studied the addition of azlactone **1** to methyl-propiolate **2** catalyzed by **cat I**. Consistent with the bifunctional activation mode of the phosphonium catalyst previously established by our⁶⁶ and Yamanaka and Ooi's work,⁵⁶ both the azlactone enolate and the propiolate were considered to be H-bonded to the catalyst's N-H groups. In addition to the reaction from each enantioface of the azlactone enolate (giving rise to enantiomeric adducts), two different orientations (*endo* and *exo*) of the propiolate relative to the azlactone, and two possible

conformations of the azlactone benzyl group (*anti* or *gauche* with respect to the forming C-C bond) were considered for each enantiomer (**Figure 3**). 8 possible TSs were considered.

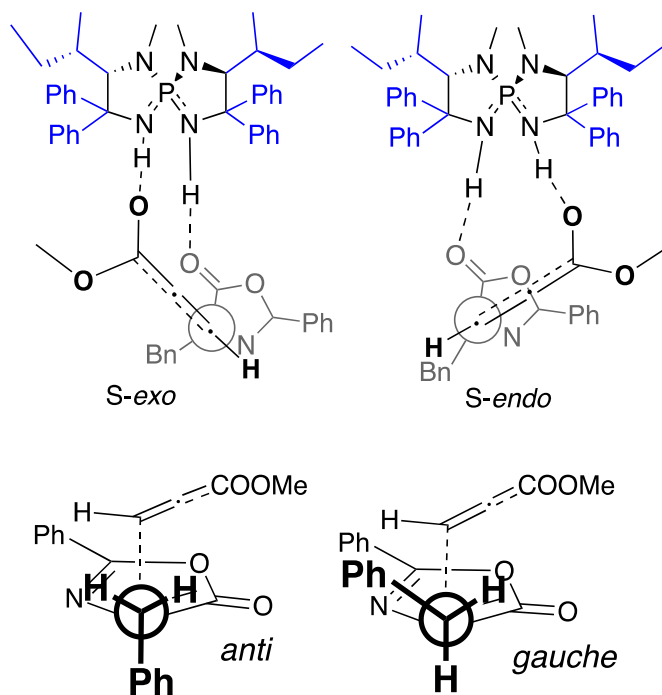


Figure 3. TS conformations considered with **cat I**; above: different orientations of reactants; below: rotamers of the azlactone.

A frontal view of this catalyst (**Figure 4**) reveals that two distal phenyl groups lie in a co-planar arrangement to create a steric barrier on either side of the iminophosphorane functionality. In the most stable TSs, the azlactone is near parallel on one side of this steric “wall”, while the alkyne is threaded through the space in-between the two phenyl rings. *Exo*-TSs are more stable than *endo*-TSs for both enantiomers, such that the latter structures barely contribute to the Boltzmann population at the reaction temperature. In the most stable (*S*)-*exo*-TS, the methyl ester and azlactone Ph-group are directed away from most hindered quadrants of the catalyst (upper-right

and lower-left of the representation in **Figure 4**), while in the (*R*)-*exo*TS a steric clash between these groups evidently destabilize it by around 1.8 kcal/mol. This rationale is congruent with the origins of asymmetric conjugate addition to other electrophiles.⁵⁶ TSs in which both propiolate and azlactone cross the central gap ((*S*)-*endo*-TS and (*R*)-*exo*-TS, both with *anti* and *gauche* benzyl conformations) were located, but are disfavored by more than 4 kcal/mol than the most stable structure (details in SI).

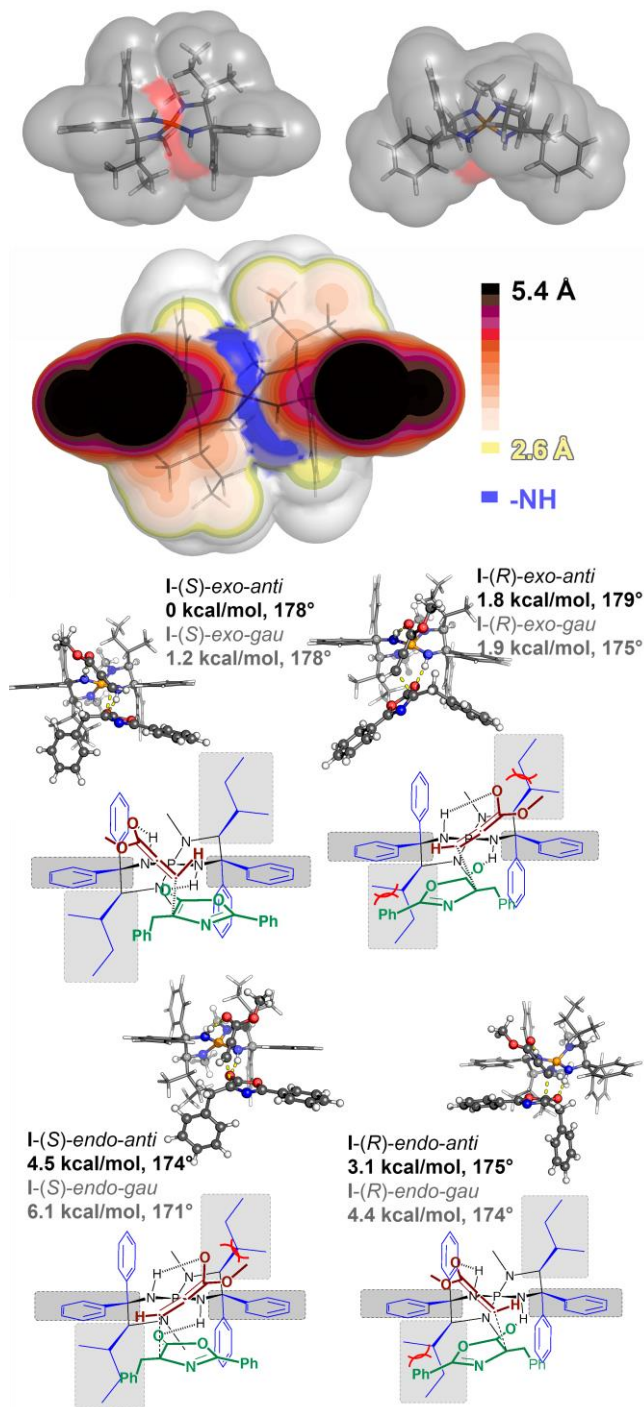


Figure 4. Above: Frontal view (left), top view (right) and steric map of the 3D Structure of **cat I**. Below: **cat I** promoted Michael addition TSs of azlactone **1** to propiolate **2**. Allenic C=C=C angles shown in degrees.

The allenolate anion and allenic enol geometries have been studied computationally by Zimmerman⁹³: although commonly drawn as the linear valence bond isomer (N.B. linear and bent forms are *not* canonical resonance forms), the gas-phase preference is for a bent allenolate geometry ($\theta_{\text{C}=\text{C}=\text{C}} = 138^\circ$). Furthermore, this preference is counter-cation dependent, varying from 117° to linear. In this reaction (**1** + **2**), we see proton transfer from **catI** to the ester O atom in the addition step to form a non-linear allenic enol intermediate. From the (*S*)-*exo*-TS, the reaction coordinate arrives at an allenic-enol (7.6 kcal/mol below the addition TS) in which the C=C=C angle is 174° ; from the (*R*)-*exo*-TS the C=C=C angle is 150° . In both cases the bending is such that the ester and azlactone groups are disposed in an (*E*)-configuration.

From the allenic enol intermediate a tautomerization step is required to form the final adduct by α -C protonation. This process can be mediated by the catalyst, for which the most stable TS leads to the (*E*)-olefin. A catalyst imino group transports the enolic proton to the α -carbon, while the other imino group remains H-bonded to the azlactone oxygen (**Figure 5**); this is the so-called “*proton slide*” mechanism.⁹⁴⁻⁹⁸ The most stable TS leading to the (*Z*)-olefin differs in that the azlactone is not H-bonded to the catalyst; instead, the catalyst iminium group protonates the substrate α -carbon, while the other imino group deprotonates the enol (“*proton relay*” mechanism^{69,99-101}). We have also found “*proton slide*” and “*proton relay*” TS tautomerization leading to *Z*- and *E*-products, respectively, but their energies are considerably higher (details in Supporting Information). The TS yielding the (*E*)-product lies 0.7 kcal/mol higher than the preceding intermediate, whereas the (*Z*)-tautomerization TS lies 2.0 kcal/mol above. Both TS structures can be accessed from the intermediate.¹⁰² This computed mechanism, in which the conversion from allenic enol to alkenyl ester dictates product configuration, is consistent with Ooi’s original hypothesis.³⁰ However, kinetic allenolate protonation typically occurs *trans*-to the

larger of the β -substituents to form the less stable (*Z*)-alkene.⁹³ We find that the *E/Z* selectivity is determined by the Gibbs energy difference between the two tautomerization TSs (0.7 vs. 2.0 kcal/mol), and that this result is consistent with experiment (22:1 *E/Z* computed vs. 17:1 experimental). C-protonation is predicted to occur much more readily than the retro-Michael process, making both steps irreversible, and so the mechanistic scenario is closest to that shown in Figure 2a. The addition step is therefore enantio-determining, giving a predicted (*S*) vs. (*R*) selectivity of 97%e.e. which is congruent with experiment (93% e.e.).

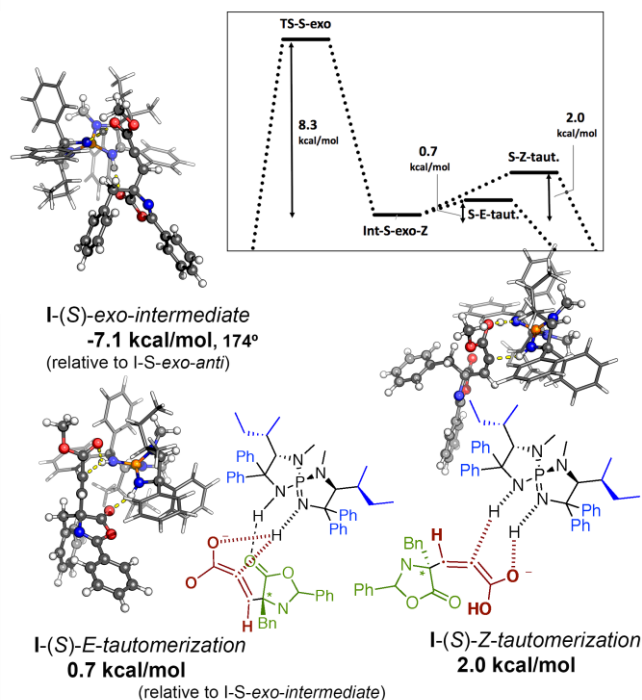


Figure 5. From the allenic enol intermediate following the (*S*)-*exo*-TS α -C protonation is mediated by **cat I**.

The reaction between 2-benzyloxythiazol-5(4 H)-one **4** and pyrazole propiolate derivative **5** (**Figure 1**) catalyzed by **cat III** proceeds via similar addition TSs. *Endo*-TSs are too high in energy (more than 9 kcal/mol) to contribute to the final product distribution; in the *exo* TSs the

alkyne is oriented axially through the central gap in the catalyst's equatorial barrier (**Figure 6**). In the most stable (*S*)-TS, the pyrazole shows a *s-cis* conformation with respect to the carbonyl group, although in the reactant ground state the *s-trans* conformation is preferred (by 2.9 kcal/mol). Previously the *s-trans* conformation was preferred for a Michael addition to a pyrazole crotonate.¹⁰³ For the most stable (*R*)-TS, the pyrazole conformation is *s-trans*. In this TS which is destabilized by 2.3 kcal/mol relative to the (*S*)-pathway, steric interactions occur with the upper-right substituents of the catalyst that are not alleviated by the change to *s-cis* conformation. Less stable TSs exist for both enantiomers in which the pyrazole configuration is inverted. As the enantiodetermining step, computed TS Gibbs energies are consistent with experiment (97% e.e. calculated vs. 93% e.e.). In all TSs the adduct shows an incipient *E* geometry, although the C=C=C angle is very close to linearity. A flat potential energy surface (PES) prevented us from characterizing the TSs for α -C protonation, but we hypothesize that, just as found earlier, both olefin geometries can be accessed with a kinetic preference for the (*E*)-configuration.

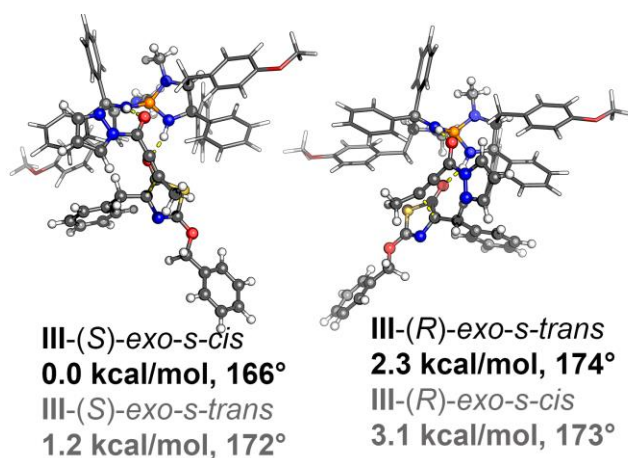


Figure 6. TSs for the addition of 2-benzyloxythiazol-5(4 H)-one **4** to pyrazol propiolate **5** derivative catalyzed by **cat III**. Allenic C=C=C angles shown in degrees.

We turned our attention to the reaction between **1** and **2** catalyzed by **cat II**. Unlike **catI** and **catIII**, there are four iminium groups that can interact with the reactants. However, as shown previously, activation modes involving two symmetry-equivalent N (both imino groups adjacent to either a diaryl- or ^tPr-substituted carbon) do not contribute towards catalysis (they are less stable by > 4 kcal/mol, details in SI). A frontal 3D-representation of the catalyst (**Figure 7**) shows that in the vicinity of the N atom attached to the isopropyl-substituted C atom, the isopropyl and the distal axial aryl group block one side of the catalyst (LHS in **Figure 7**). The volume of these groups is so large that all TSs in which the bulkier azlactone H-bonds to this N atom are less stable, not contributing to the final product distribution (lying more than 3 kcal/mol above the most stable TS). For the remaining addition TSs, in II-(*R*)-*endo* and II-(*S*)-*exo* the methyl ester of the propiolate is directed toward the bulkier side, and accordingly also show a high relative energy. II-(*S*)-*endo* and II-(*R*)-*exo* TSs do not have this problem. In the most stable II-(*S*)-*endo* TS, the more flexible benzyl group is directed to the bulkier side, but can rotate to alleviate steric interactions. In the II-(*R*)-*exo* TS, the rigid azlactone Ph-group cannot twist away, and both reactants rotate with respect to the iminophosphorane, leading to a higher (0.9 kcal/mol) energy. The computed enantioselectivity (84% e.e.) is again consistent with experiment (90%e.e.).

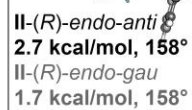
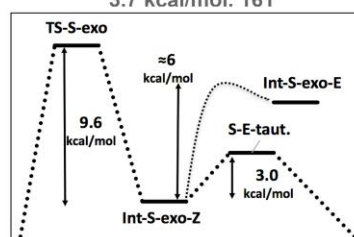
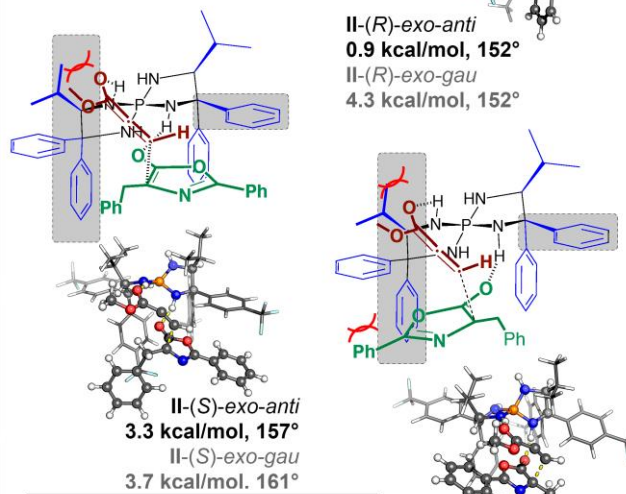
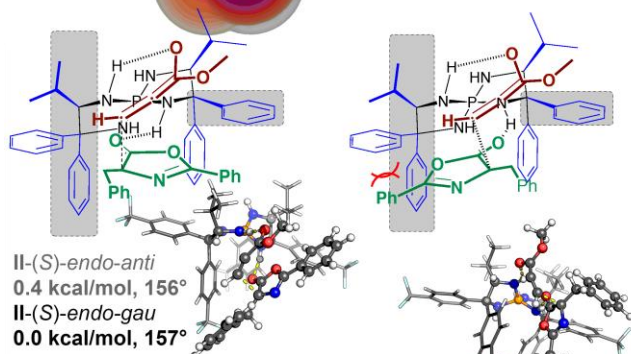
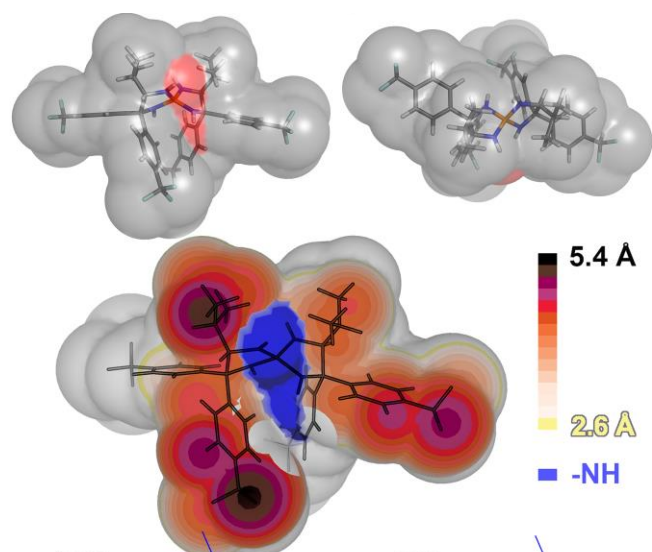


Figure 7. Above: Frontal view (left), top view (right) and steric map of the 3D Structure of **cat II**. Below: Addition TSs for the reaction between azlactone **1** and propiolate **2** catalyzed by **cat II**. Allenic C=C=C angles shown in degrees.

The difference in the allenic C=C=C angle in addition TSs computed for **cat II** (Figure 7) and for **cat I** (Figure 4) is notable. For **cat I** there is a modest deviation from linearity (174 – 179°) towards an (*E*)-configuration, whereas for **cat II**, the C=C=C angle is more bent (152 – 161°) and shows a clear (*Z*)-configuration. This C=C=C difference is more marked in the allenyl enol intermediate structures: 143° for (*S*)-*endo* and 147° for (*R*)-*exo* intermediates, in both cases corresponding to a (*Z*)-configuration. With this catalyst the intermediates are non-linear, and we find a large energy gap (≈ 7 kcal/mol)¹⁰⁴ between bent allenyl enol intermediates with (*Z*) and (*E*)-configurations, with the (*Z*)-configuration being the more stable. This energy gap is much higher than barrier for the catalyst-promoted tautomerization TS (3.0 kcal/mol), such that these distinct vinyl anion configurations do not interconvert. This explains the absence of (*E*)-product: the (*Z*)-allenyl enol intermediate undergoes C-protonation faster than isomerization to (*E*)-allenyl enol. This mechanistic scenario is described by Figure 2c: Michael addition occurs irreversibly and is both enantio- and diastereo-determining since the alkene stereochemistry is also set in this step.

The TSs for Michael addition with **cat I** and **cat II** differ in terms of the forming allenyl intermediate. With **cat I**, which favors (*E*)-alkene formation, the geometry in the TS is close to linear, with a slight (*E*)-configuration. With **cat II**, which favors (*Z*)-alkene formation, the

C=C=C angle is more acute and adopts a (*Z*)-configuration. The main difference between both catalysts is the disposition of the bulky substituents around the catalytic iminophosphorane group. Therefore, we decided to repeat the calculations for the reaction between **1** and **2** with a model catalyst in which the four phenyl groups of **cat I** were substituted by H atoms. To our surprise, in all cases the C=C=C angle in the addition TS was reduced to 163°-158° (depending on the structure, details in SI) with the allenyl enol showing a (*Z*)-geometry.

Consideration of the reaction between **1** and cyanoacetylene **3** catalyzed by **cat I** also provides insight into the origins of the *Z/E* selectivity. The H-bond between the catalyst and the nitrile Nitrogen atom is, unlike in the propiolactone, co-linear with the triple bond. This small difference results in the impossibility, despite several attempts, of finding addition TSs corresponding to the *endo*-orientation between the reactants. It was, however, possible to find TSs leading to (*R*)- and (*S*)-products in which both the cyanoacetylene and the azlactone “cross” the aperture between the equatorial catalyst phenyl rings although these are less stable. As with the propiolate reaction, in the most stable TSs the azlactone lies on one side of the equatorial aromatic rings and the cyanoacetylene passes through the gap (**Figure 8**). The energy difference between (*S*)- and (*R*)- TSs (1.1 kcal/mol, also in good agreement with the experimental results: 90 vs. 97% e.e.) can be explained because in the (*S*)-TS, the more flexible benzyl group of the azlactone (and not the rigid phenyl group) occupies the lower-left more voluminous “quadrant” of the catalyst, where a sec-butyl group is located. But again, the most notable feature is the C=C=C *Z* angle of the allenyl enol (156°-157°), that is reduced further to 131°-135° in the intermediates). Comparing the TS geometries with propiolate and cyanoacetylene shows that in the former, the methyl ester groups rest over the equatorial catalyst’s phenyl rings, which prevents the allenyl enol from adopting a (*Z*)-configuration. The smaller cyanoacetylene does not

have this problem, and therefore, in the absence of a more severe steric interaction the (*Z*)-geometry is preferred. The formation of the (*Z*)-alkene is a consequence of the Michael addition step, which forms an allenyl enol intermediate with a pronounced (*Z*)-geometry for which protonation is much faster than interconversion to the (*E*)-form.

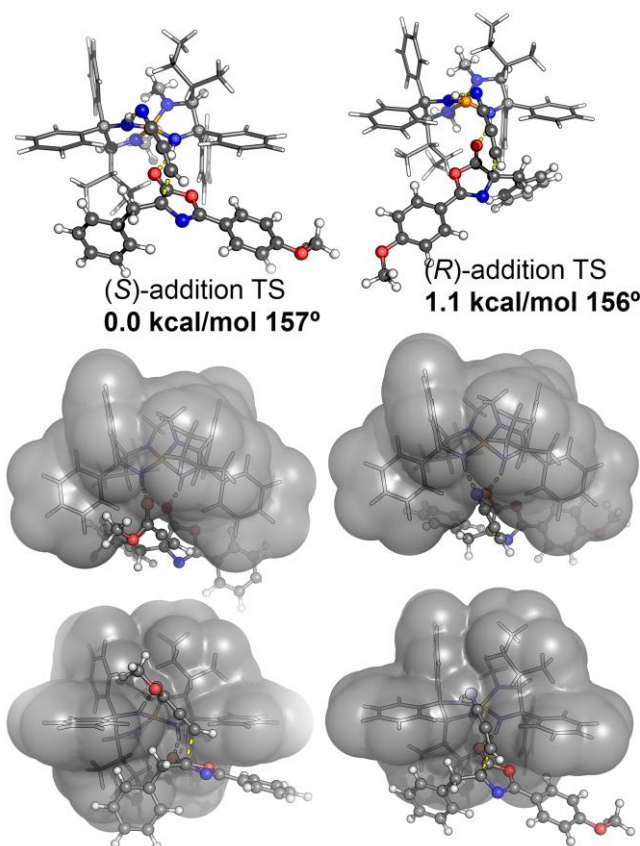


Figure 8. Above: Addition TSs for the reaction between the azlactone **1** and cyanoacetylene **3** catalyzed by **cat I**. Below, comparison of TSs with propiolate (left) and cyanoacetylene (right) electrophiles.

The above results reveal the ability of **cat I** and **cat III** to prevent the formation of the (*Z*)-allenyl enol intermediate by steric effects provided the electrophile is sufficiently bulky. However, in the absence of these steric effects, why is there an intrinsic preference for a (*Z*)-like addition TS? To

account for this observation, we studied the PES for the uncatalyzed *exo* addition of azlactone **1** enolate to methyl propiolate **2** (**Figure 9**). The azlactone benzyl substituent was replaced by a methyl group. We scanned over two coordinates: the C=C=C angle and the forming C-C distance. At large C-C separations, the minimum energy path corresponds to a linear (C=C=C angle $\approx 180^\circ$). As the reactants pass through the TS region, the minimum energy path moves towards a *Z*-configuration; downstream from the TS, two minima appear: one corresponding to the *Z* and one to the *E* bent vinyl carbanion (allenolate). The preference for the (*Z*)-geometry during early stages of the C-C bond formation might be reminiscent from the geometry of the LUMO of the methyl propiolate, that shows a node between the alkynyl carbon atoms. Due to this node, the new C-C bond and electronic lone pair are “*anti*”, implying that the azlactone and the methyl ester are on the same side (*Z*).

The barrier that separates these product minima is small (< 5 kcal/mol) compared to the values calculated for isomerization of the intermediates with **cat II**. However, a similar scan for the *endo*-addition reveals a stronger preference for the (*Z*)-configured anion, and a larger barrier for interconversion to the (*E*)-form. This is due to secondary nonbonding interactions between the π -systems of the azlactone and the allene. As shown in Figure 9, the 0.5 a.u. isosurface of the reduced density gradient shows a region where the second eigenvalue of the density hessian matrix is negative (shown in green in Figure 9), which corresponds to a stabilizing interaction⁸⁸. **Cat II** not only allows for exclusive formation of the (*Z*)-configured allenyl enol, but also prevents its isomerization to the (*E*)-form, since steric effects induce a preference for the *endo* TS.

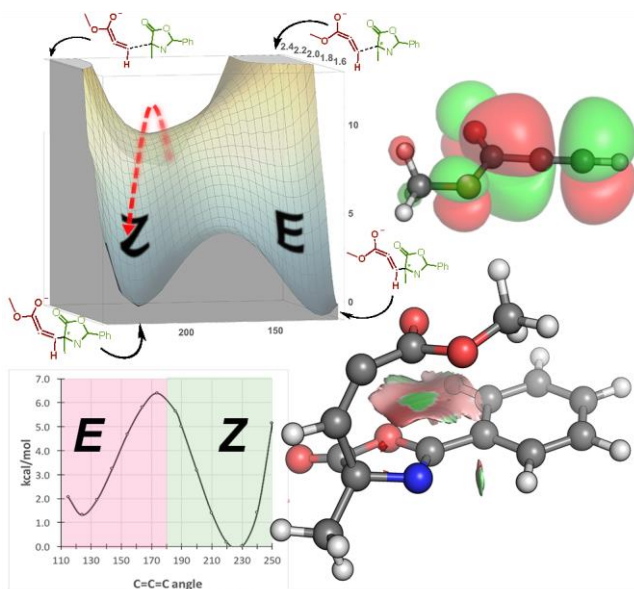


Figure 9. Above, left: PES for the addition of azlactone enolate to methyl propiolate; right: LUMO of the methyl propiolate. Below, left: relaxed scan of the C=C=C angle for the *endo* allene enolate; right: NCI isosurface for the (*Z*)-configured allenolate; a stabilizing nonbonding interaction is shown by the green surface between ester and azlactone.

Conclusions

Using ONIOM(QM/MM) calculations, iminophosphorane catalyzed additions of azlactones have been found to proceed via allenyl intermediates with geometries ranging from linear (i.e. allene-like) to bent (i.e. vinyl anion-like). In the absence of steric constraints, we found an innate kinetic preference for the formation of bent (*Z*)-configured intermediates in the Michael addition step.

Protonation of these intermediates at the α -C is faster than *Z-E* isomerization and so the (*Z*)-configured alkene dominates. In contrast, a kinetic preference for the (*E*)-alkene can arise from the stereoselective α -C protonation in reactions proceeding via a linear allenyl intermediate.

In the reaction between azlactone **1** and methyl propiolate **2** catalyzed by **cat I**, and probably also for the reactions between 2-benzyloxythiazol-5(4 H)-one **4** and the pyrazole propiolate derivative **5** catalyzed by **cat III**, a linear allenyl enol is formed in the enantio-determining addition step. Subsequent protonation at the α -C is diastereo-determining and the stabilities of these tautomerization TSs agree well with experimental levels of (*E*)-selectivity. In the reaction between **1** and **2** catalyzed by **Cat II**, however, steric interactions between the catalyst and the substrate are not properly positioned to prevent formation of the (*Z*)-allene enol. This intermediate undergoes α -C protonation faster than it can interconvert to an (*E*)-geometry, which accounts for the absence of (*E*)-olefin in the product distribution. The Michael addition step thus becomes both enantio- and distereo-determining in this case.

In the reaction of smaller electrophiles such as cyanoacetylene **3**, or by constructing a model catalyst without bulky flanking groups, we have confirmed the tendency for a (*Z*)-configured intermediate in the absence of more severe steric effects. Protonation leads to a (*Z*)-olefin faster than *Z/E* allene enol isomerization. Kinetically-controlled formation of the (*E*)-alkene in this case is therefore the exception, and not the rule. The success of iminophosphorane catalysts in promoting the formation of the (*E*)-product results from its ability to use steric interactions to overcome an innate stereoelectronic preference for (*Z*)-allenyl intermediates which rapidly protonate. Understanding the role of non-linear allenyl enol intermediates in the formation of

alkenes from alkynes will be important for the development of stereoselective catalytic methodologies in future.

ASSOCIATED CONTENT

Supporting Information. Full list of authors in ref. 57. Procedure for the preparation of the steric maps in Figures 4 and 7. Comparison between ONIOM(QM:MM) and M062X/6-31G(d,p) energies. Comparison between ONIOM(M06-2X/6-31G(d,p):UFF) and M062X/6-31G(d,p) geometries. Cartesian coordinates of all optimized TS and intermediates. The following files are available free of charge.

ACKNOWLEDGMENT

We acknowledge the employment of University of Salamanca server housing service. We thank A. López García and J. A. González Ramos for IT support. RSP acknowledges the use of the EPSRC National Service for Computational Chemistry Software at Imperial College London in carrying out this work. The picture from: <https://www.goodfreephotos.com/vector-images/you-shall-not-pass-sign-with-gandalf-vector-clipart.png.php>, under the CC0 / Public Domain Lincense, was used for the preparation of the TOC graphics.

REFERENCES

- (1) Scheffler, U.; Mahrwald, R. *Chem.--Eur. J.* **2013**, *19*, 14346-14396.

- (2) Wang, Y.-Y.; Kanomata, K.; Korenaga, T.; Terada, M. *Angew. Chem. Int. Ed.* **2015**, *55*, 927-931.
- (3) Dong, N.; Zhang, Z.-P.; Xue, X.-S.; Li, X.; Cheng, J.-P. *Angew. Chem. Int. Ed.* **2015**, *55*, 1460-1464.
- (4) Chen, S.; Lou, Q.; Ding, Y.; Zhang, S.; Hu, W.; Zhao, J. *Adv. Synth. Catal.* **2015**, *357*, 2437-2441.
- (5) Cao, D.; Zhang, J.; Wang, H.; Zhao, G. *Chem.--Eur. J.* **2015**, *21*, 9998-10002.
- (6) Sánchez-Roselló, M.; Mulet, C.; Guerola, M.; del Pozo, C.; Fustero, S. *Chem.--Eur. J.* **2014**, *20*, 15697-15701.
- (7) Phelan, J. P.; Patel, E. J.; Ellman, J. A. *Angew. Chem. Int. Ed.* **2014**, *53*, 11329-11332.
- (8) Murai, K.; Fukushima, S.; Hayashi, S.; Takahara, Y.; Fujioka, H. *Org. Lett.* **2010**, *12*, 946-966.
- (9) Hoashi, Y.; Okino, T.; Takemoto, Y. *Angew. Chem. Int. Ed.* **2005**, *44*, 4032-4035.
- (10) Okino, T.; Hoashi, Y.; Takemoto, Y. *J. Am. Chem. Soc.* **2003**, *125*, 12672-12673.
- (11) Simón, L.; Muñiz, F. M.; Sáez, S.; Raposo, C.; Morán, J. R. *Eur. J. Org. Chem.* **2007**, *2007*, 4821-4830.
- (12) Martínez, J. I.; Villar, L.; Uria, U.; Carrillo, L.; Reyes, E.; Vicario, J. L. *Adv. Synth. Catal.* **2014**, *356*, 3627-3648.
- (13) Loh, C. C. J.; Chauhan, P.; Hack, D.; Lehmann, C.; Enders, D. *Adv. Synth. Catal.* **2014**, *356*, 3181-3186.
- (14) Sanchez Duque, M. d. M.; Baslé, O.; Génisson, Y.; Plaquevent, J.-C.; Bugaut, X.; Constantieux, T.; Rodriguez, J. *Angew. Chem. Int. Ed.* **2013**, *52*, 14143-14146.
- (15) Loh, C. C. J.; Atodiresei, I.; Enders, D. *Chem.--Eur. J.* **2013**, *19*, 10822-10826.
- (16) Tan, B.; Hernández-Torres, G.; Barbas, C. F. *Angew. Chem. Int. Ed.* **2012**, *51*, 5381-5385.
- (17) Bandar, J. S.; Lambert, T. H. *J. Am. Chem. Soc.* **2012**, *134*, 5552-5555.
- (18) Yang, H.; Wong, M. W. *J. Org. Chem.* **2011**, *76*, 7399-7405.
- (19) Lv, J.; Zhang, L.; Zhou, Y.; Nie, Z.; Luo, S.; Cheng, J.-P. *Angew. Chem. Int. Ed.* **2011**, *50*, 6610-6614.
- (20) Fraile, A.; Parra, A.; Tortosa, M.; Alemán, J. *Tetrahedron* **2014**, *70*, 9145-9173.
- (21) Bella, M.; Jørgensen, K. A. *J. Am. Chem. Soc.* **2004**, *126*, 5672-5673.
- (22) Mola, L.; Font, J.; Bosch, L.; Caner, J.; Costa, A. M.; Etxebarria-Jardi, G.; Pineda, O.; de Vicente, D.; Vilarrasa, J. *J Org Chem* **2013**, *78*, 5832-5842.
- (23) Tejedor, D.; Álvarez-Méndez, S. J.; López-Soria, J. M.; Martín, V. S.; García-Tellado, F. *Eur. J. Org. Chem.* **2014**, *2014*, 198-205.
- (24) Evans, P. A.; Murthy, V. S.; Roseman, J. D.; Rheingold, A. L. *Angew. Chem. Int. Ed.* **1999**, *38*, 3175-3177.
- (25) Fan, Y. C.; Kwon, O. *Org. Lett.* **2012**, *14*, 3264-3267.
- (26) Lan, Q.; Wang, X.; Maruoka, K. *Tetrahedron Lett.* **2007**, *48*, 4675-4678.
- (27) Wang, X.; Kitamura, M.; Maruoka, K. *J. Am. Chem. Soc.* **2007**, *129*, 1038-1039.
- (28) Lan, Q.; Wang, X.; Shirakawa, S.; Maruoka, K. *Org. Process. Res. Dev.* **2010**, *14*, 684-686.
- (29) Misaki, T.; Kawano, K.; Sugimura, T. *J Am Chem Soc* **2011**, *133*, 5695-5697.
- (30) Kang, Q.; Zhao, Z.-A.; You, S.-L. *Org. Lett.* **2008**, *10*, 2031-2034.
- (31) Uraguchi, D.; Ueki, Y.; Sugiyama, A.; Ooi, T. *Chem. Sci.* **2013**, *4*, 1308-1311.

- (32) Uraguchi, D.; Yamada, K.; Ooi, T. *Angew Chem Int Ed Engl* **2015**, *54*, 9954-9957.
- (33) Krawczyk, H.; Dziegielewski, M.; Deredas, D.; Albrecht, A.; Albrecht, L. *Chem.-Eur. J.* **2015**, *21*, 10268-10277.
- (34) Uraguchi, D.; Sakaki, S.; Ooi, T. *J. Am. Chem. Soc.* **2007**, *129*, 12392-12393.
- (35) Uraguchi, D.; Nakamura, S.; Ooi, T. *Angew. Chem. Int. Ed.* **2010**, *49*, 7562-7565.
- (36) Uraguchi, D.; Nakamura, S.; Sasaki, H.; Konakade, Y.; Ooi, T. *Chem. Commun.* **2014**, *50*, 3491-3493.
- (37) Nuñez, M. G.; Farley, A. J. M.; Dixon, D. J. *J. Am. Chem. Soc.* **2013**, *135*, 16348-16351.
- (38) Goldys, A. M.; Núñez, M. G.; Dixon, D. J. *Org. Lett.* **2014**, *16*, 6294-6297.
- (39) Uraguchi, D.; Ito, T.; Nakamura, S.; Ooi, T. *Chem. Sci.* **2010**, *1*, 488-490.
- (40) Horwitz, M. A.; Zavesky, B. P.; Martinez-Alvarado, J. I.; Johnson, J. S. *Org. Lett.* **2015**, *18*, 36-39.
- (41) Dixon, D.; Robertson, G.; Farley, A. *Synlett* **2016**, *27*, 21-24.
- (42) Farley, A. J.; Sandford, C.; Dixon, D. J. *J Am Chem Soc* **2015**, *137*, 15992-15995.
- (43) Uraguchi, D.; Ueki, Y.; Ooi, T. *J. Am. Chem. Soc.* **2008**, *130*, 14088-14089.
- (44) Uraguchi, D.; Ueki, Y.; Ooi, T. *Chem. Sci.* **2012**, *3*, 842-845.
- (45) Uraguchi, D.; Yoshioka, K.; Ueki, Y.; Ooi, T. *J. Am. Chem. Soc.* **2012**, *134*, 19370-19373.
- (46) Kondoh, A.; Oishi, M.; Takeda, T.; Terada, M. *Angew Chem Int Ed Engl* **2015**, *54*, 15836-15839.
- (47) Takeda, T.; Kondoh, A.; Terada, M. *Angew Chem Int Ed Engl* **2016**, *55*, 4734-4737.
- (48) Ohmatsu, K.; Ando, Y.; Ooi, T. *J. Am. Chem. Soc.* **2013**, *135*, 18706-18709.
- (49) Gao, X.; Han, J.; Wang, L. *Org Lett* **2015**, *17*, 4596-4599.
- (50) Gao, X.; Han, J.; Wang, L. *Org. Chem. Front.* **2016**, *3*, 656-660.
- (51) Takeda, T.; Terada, M. *J. Am. Chem. Soc.* **2013**, *135*, 15306-15309.
- (52) Brak, K.; Jacobsen, E. N. *Angew. Chem. Int. Ed.* **2012**, *52*, 534-561.
- (53) Paton, R. S. *Org. Biomol. Chem.* **2014**, *12*, 1717-1720.
- (54) Johnston, C. P.; Kothari, A.; Sergeieva, T.; Okovytyy, S. I.; Jackson, K. E.; Paton, R. S.; Smith, M. D. *Nat Chem* **2015**, *7*, 171-177.
- (55) Simón, L.; Paton, R. S. *J. Org. Chem.* **2015**, *80*, 2756-2766.
- (56) Yamanaka, M.; Sakata, K.; Yoshioka, K.; Uraguchi, D.; Ooi, T. *J Org Chem* **2016**.
- (57) Frisch, M. J.; al., e.; , Gaussian, Inc.: Wallingford CT, 2009.
- (58) Svensson, M.; Humbel, S.; Morokuma, K. *J. Chem. Phys.* **1996**, *105*, 3654-3661.
- (59) Dapprich, S.; Komáromi, I.; Byun, K. S.; Morokuma, K.; Frisch, M. J. *J. Mol. Str.* **1999**, *461*, 1-21.
- (60) Vreven, T.; Morokuma, K. *J. Comput. Chem.* **2000**, *21*, 1419-1432.
- (61) Peng, Q.; Duarte, F.; Paton, R. S. *Chem. Soc. Rev.* **2016**, *45*, 6093-6107.
- (62) Zhao, Y.; Truhlar, D. *Theor Chem Account* **2008**, *120*, 215-241.
- (63) Zhao, Y.; Truhlar, D. G. *Acc. Chem. Res.* **2008**, *41*, 157-167.
- (64) Krishnan, R.; Binkley, J. S.; Seeger, R.; Pople, J. A. *J. Chem. Phys.* **1980**, *72*, 650-654.

- (65) Gill, P. M. W.; Johnson, B. G.; Pople, J. A.; Frisch, M. J. *Chem. Phys. Lett.* **1992**, *197*, 499-505.
- (66) Rappé, A. K.; Casewit, C. J.; Colwell, K. S.; Goddard III, W. A.; Skid, W. M. *J. Am. Chem. Soc.* **1992**, *114*, 10024-10035.
- (67) Simón, L.; Goodman, J. M. *J. Am. Chem. Soc.* **2008**, *130*, 8741-8747.
- (68) Simón, L.; Goodman, J. M. *J. Org. Chem.* **2011**, *76*, 1775-1788.
- (69) Simón, L.; Goodman, J. M. *J. Am. Chem. Soc.* **2012**, *134*, 16869-16876.
- (70) Simón, L.; Goodman, J. M. *J. Org. Chem.* **2010**, *75*, 589-597.
- (71) Simón, L.; Goodman, J. M. *J. Am. Chem. Soc.* **2009**, *131*, 4070-4077.
- (72) Grayson, M. N.; Pellegrinet, S. C.; Goodman, J. M. *J. Am. Chem. Soc.* **2012**, *134*, 2716-2722.
- (73) Reid, J. P.; Simón, L.; Goodman, J. M. *Acc Chem Res* **2016**, *49*, 1029-1041.
- (74) Simón, L.; Paton, R. S. *Org Biomol Chem* **2016**, *14*, 3031-3039.
- (75) Simón, L.; Goodman, J. M. *Org. Biomol. Chem.* **2011**, *9*, 689-700.
- (76) In testing, DFT-D optimized ion-pair structures compare favorably against the results of molecular dynamics simulations explicitly solvated by toluene.
- (77) Clark, T.; Chandrasekhar, J.; Schleyer, P. v. R. *J. Comput. Chem.* **1983**, *4*, 294-301.
- (78) Cammi, R.; Mennucci, B.; Tomasi, J. *J. Phys. Chem. A* **1999**, *103*, 9100-9108.
- (79) Cammi, R.; Mennucci, B.; Tomasi, J. *J. Phys. Chem. A* **2000**, *104*, 5631-5637.
- (80) Cossi, M.; Rega, N.; Scalmani, M.; Barone, V. *J. Chem. Phys.* **2001**, *114*, 5691-5701.
- (81) Cossi, M.; Scalmani, G.; Rega, N.; Barone, V. *J. Chem. Phys.* **2002**, *117*, 43-54.
- (82) Cossi, M.; Scalmani, G.; Rega, N.; Barone, V. *J. Comput. Chem.* **2003**, *24*, 669-681.
- (83) A. V. Marenich; C. J. Cramer; D. G. Truhlar. *Phys. Chem. B* **2009**, *113*, 6378-6396.
- (84) Grimme, S. *Chem.--Eur. J.* **2012**, *18*, 9955-9964.
- (85) Funes-Adois, I.; R. Paton GoodVibes v1.0.1, 2016. doi:<http://dx.doi.org/10.5281/zenodo.60811> (accessed 29th December 2016).; (b) this approach produces Gibbs energies which correlate more closely with experiment than alternative quasi-harmonic corrections: Luccarell, J.; Jackson, K. E.; Hamilton, A. D.; Paton, R. S. *in preparation*
- (86) *The PyMOL Molecular Graphics System, Version 0.99, Schrödinger, LLC.*
- (87) Johnson, E. R.; Keinan, S.; Mori-Sánchez, P.; Contreras-García, J.; Cohen, A. J.; Yang, W. *J. Am. Chem. Soc.* **2010**, *132*, 6498-6506.
- (88) Contreras-García, J.; Johnson, E. R.; Keinan, S.; Chaudret, R.; Piquemal, J.-P.; Beratan, D. N.; Yang, W. *J. Chem. Theory Comput.* **2011**, *7*, 625-632.
- (89) Skara, G.; Pinter, B.; Top, J.; Geerlings, P.; De Proft, F.; De Vleeschouwer, F. *Chem.--Eur. J.* **2015**, *21*, 5510-5519.
- (90) Falivene, L.; Credendino, R.; Poater, A.; Petta, A.; Serra, L.; Oliva, R.; Scarano, V.; Cavallo, L. *Organometallics* **2016**, *35*, 2286-2293.
- (91) Poater, A.; Ragone, F.; Mariz, R.; Dorta, R.; Cavallo, L. *Chemistry* **2010**, *16*, 14348-14353.
- (92) Liu, P.; Montgomery, J.; Houk, K. N. *J Am Chem Soc* **2011**, *133*, 6956-6959.
- (93) Zimmerman, H. E.; Pushechnikov, A. *Eur. J. Org. Chem.* **2006**, *2006*, 3491-3497.
- (94) Bruice, P. Y.; Bruice, T. C. *J. Am. Chem. Soc.* **1974**, *96*, 5533-5542.

- (95) Cannizzaro, C. E.; Strassner, T.; Houk, K. N. *J. Am. Chem. Soc.* **2001**, *123*, 2668-2669.
- (96) Martinelli, E.; Vicini, A. C.; Mancinelli, M.; Mazzanti, A.; Zani, P.; Bernardi, L.; Fochi, M. *Chem. Commun.* **2015**, *51*, 658-660.
- (97) Simón, L.; Muñoz, F. M.; Sáez, S.; Raposo, C.; Morán, J. R. *Eur. J. Org. Chem.* **2008**, 2397-2403.
- (98) Gammack Yamagata, A. D.; Datta, S.; Jackson, K. E.; Stegbauer, L.; Paton, R. S.; Dixon, D. J. *Angew Chem Int Ed Engl* **2015**, *54*, 4899-4903.
- (99) Guo, W.; González-Fabra, J.; Bandeira, N. A. G.; Bo, C.; Kleij, A. W. *Angew. Chem. Int. Ed.* **2015**, *54*, 11686-11690.
- (100) Simón, L.; Goodman, J. M. *J. Org. Chem.* **2007**, *72*, 9656-9662.
- (101) Chuma, A.; Horn, H. W.; Swope, W. C.; Pratt, R. C.; Zhang, L.; Lohmeijer, B. G. G.; Wade, C. G.; Waymouth, R. M.; Hedrick, J. L.; Rice, J. E. *J. Am. Chem. Soc.* **2008**, *130*, 6749-6754.
- (102) Attempts to find a TS corresponding to the Z/E isomerization of the allenolate intermediates failed, but relaxed scan calculations (in which C=C=C angle was fixed and scanned while the rest of internal coordinates were optimized) show that the energy increases monotonously from the (S)-exo intermediate to (Z)-allenolate structures. The energy difference is small (<2 kcal/mol from the intermediate), indicating that the 2.0 kcal/mol tautomerization TS can be accessed from the intermediate.
- (103) Simón, L.; Goodman, J. M. *Org. Biomol. Chem.* **2009**, *7*, 483-487.
- (104) Attempts to find the (E)-allenyl enol intermediate failed. The ≈6.7 kcal/mol energy gap correspond to the electronic energy difference between the (Z)-allenyl enol intermediate and an optimized structure in which the C=C=C angle was fixed to 150° towards the (E) configuration.

TABLE OF CONTENTS GRAPHIC

